



ORIGINAL RESEARCH ARTICLE

Surface Topography in Peripheral Milling of Ti-6Al-4V: Multi-scale Evaluation and Fractal Analysis

Dong Yang and Tianhao Jia

Submitted: 24 September 2023 / Revised: 5 November 2023 / Accepted: 9 December 2023

Ti-6Al-4V alloy has been widely used in aerospace and other fields with its excellent mechanical properties, but its poor machinability makes the surface quality difficult to control, which is reflected in multi-scale surface topography features. The peripheral milling-induced surface topography of Ti-6Al-4V was evaluated by statistical and fractal analyses methods at different scales. Firstly, the macro- and microdefects characteristics of the machined surface and their formation mechanisms were clarified. And then, the response laws of profile, height and spatial surface roughness and fractal characteristics with peripheral milling parameters (spindle speed n , radial depth of cut a_e , and feed rate f) at different scales were revealed. The results show that the natural defects are distinguished by larger-scale features, such as feeding marks and scratches, whereas the random defects are smaller-scale features, including adhered particles, random scratches, and cracks. Lower arithmetical mean deviation and maximum height are obtained at $n = 900$ rev/min, $a_e = 0.5$ mm, and $f = 0.06$ mm/rev, at the observation scales of $200 \times$ and $400 \times$. And all surface roughness parameters showed high variability at $1000 \times$. The kurtosis and skewness of the peripheral milling surface show that there are no extreme peaks and valleys. A larger fractal dimension was obtained at $n = 1150$ rev/min, $a_e = 0.3$ mm, and $f = 0.06$ mm/rev, due to surface defects making the surface structure more complex. The variation trend of the fractal characteristics, including irregularity and self-similarity, on the Ti-6Al-4V alloy surface with peripheral milling parameters is independent of the observation scale, equipment resolution, and sampling length.

Keywords fractal analysis, peripheral milling, surface roughness, surface topography, Ti-6Al-4V

1. Introduction

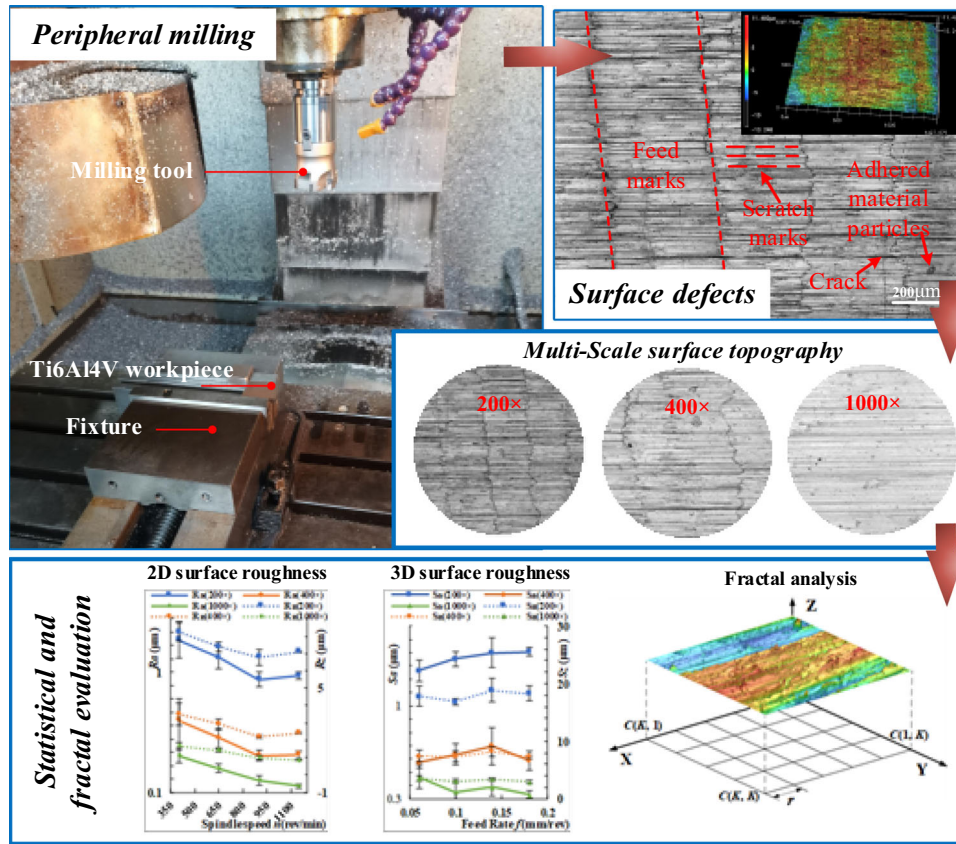
Titanium alloy Ti-6Al-4V has been widely used in the field of aerospace, biomedicine, petrochemical industry, nuclear power equipment, etc., due to its excellent properties such as high specific strength (a measure of strength equivalent to the yield strength divided by the material density), good corrosion resistance, and high thermal strength (Ref 1, 2). In order to process titanium alloy structural components with various types of surfaces, such as small planes, grooves and die lands, method of peripheral milling is always used (Ref 3-5). Nevertheless, Ti-6Al-4V is considered a typical difficult-to-machine material because of high cutting temperature, large cutting force, easy tool wear, and so on (Ref 6). As a result, it becomes challenging to control the machined surface integrity of Ti-6Al-4V. The surface topography after peripheral milling is an important indicator of surface integrity and contains complex information such as roughness, waviness, shape error, etc. And it is an important index to measure product performance, which directly affects the accuracy, surface finish, thermal conductivity, and service life of the workpiece (Ref 7,

8), and ultimately affects the overall reliability and safety of the equipment (Ref 9). Karmiris-Obratański et al. (Ref 10) studied the effects of milling process and cooling methods on surface topography and found that the surfaces produced in most cases contains high peaks with irregular features and are probable to exhibit high friction coefficient and wear as well as relatively low fluid retention capability. Molnar et al. (Ref 11) conducted hard turning and grinding experiments for hardened surfaces and quantitatively evaluated the surface topography of different sizes under different processing parameters with surface texture parameters. The application environment of titanium alloy (Ti-6Al-4V) puts forward a high requirement of surface quality induced by peripheral milling. Consequently, the quantitative analysis of the surface topography of Ti-6Al-4V alloy in peripheral milling is extremely important.

The formation of surface topography in peripheral milling depends on various factors, such as cutting parameters, workpiece and tool materials, and tool wear, among which the selection of cutting parameters is the most critical (Ref 12). Sur et al. (Ref 4) studied the Ti-6Al-4V alloy surface roughness R_a at different cutting speeds V_c and feed rates f by carrying out peripheral milling experiments with carbide end mills. Results show that the arithmetical mean deviation R_a is reduced by 24.07% at the cutting speed of $V_c = 108$ m/min ($R_a = 0.324 \mu\text{m}$) compared with $V_c = 48$ m/min ($R_a = 0.402 \mu\text{m}$). Similarly, surface roughness R_a decreases by 26.67% at $f = 0.04$ mm/tooth compared to $f = 0.06$ mm/tooth. It can be seen that the surface quality is improved at higher cutting speed and lower feed rate. Ekici et al. (Ref 13) studied the influence of milling parameters on roughness R_q of Ti-6Al-4V by using carbide tools. The results show that R_q increases with the

Dong Yang and Tianhao Jia, Department of Mechanical Engineering, Anhui University, Hefei 230601, People's Republic of China. Contact e-mail: yangdong@ahu.edu.cn.

Graphical Abstract



increase of cutting speed V_c and decreases first and then increases with the increase in feed rate f . The minimum surface roughness ($R_a = 0.196 \mu\text{m}$) can be obtained under the conditions of $V_c = 45 \text{ m/min}$ and $f = 0.09 \text{ mm/rev}$. Daniyan et al. (Ref 14) studied the effects of cutting speed (250-270 m/min), feed per tooth (0.05-0.30 mm/tooth), and axial depth of cut (0.5-3.0 mm) on Ti-6Al-4V alloy surface roughness (R_a , R_z , and R_q) and conducted milling experiments using solid milling tools. The results show that the machining parameters which result in the minimum surface roughness (R_a : $0.035 \mu\text{m}$, R_z : $1.12 \mu\text{m}$, R_q : $0.277 \mu\text{m}$) were: cutting speed (265 m/min), feed per tooth (0.05 mm), and axial depth of cut (0.5 mm). Bandapalli et al. (Ref 15, 16) conducted high-speed milling experiments on Ti-6Al-4V alloy at different spindle speed, feed rate, and depth of cut. The results show that the most influential factor was feed rate followed by depth of cut and finally by spindle speed on surface roughness R_a . In addition, they also used R_a to characterize the surface topography of titanium (grade-2) (Ref 17) and near-alpha titanium alloy (Ref 18) in high-speed milling, and concluded that feed rate was the most influential factor.

However, the profile and height roughness parameters strongly depend on the direction of measurement. The characteristics of machined surface topography are not only concentrated in the feed direction but also perpendicular to it (Ref 19). Therefore, it is essential to provide a spacial and comprehensive description of the machined surface topography. Lizzul et al.

(Ref 20) carried out milling experiments for Ti-6Al-4V alloy with different cutting speeds V_c (30 mm/min, 60 mm/min) and feed rates per tooth f_z (0.01 mm/tooth, 0.05 mm/tooth) and calculated S_a , S_{ku} (the kurtosis), S_{sk} (the skewness), S_{dq} (the root-mean-square gradient), etc. The results show that the influence of f_z on S_a , S_{ku} , S_{sk} and S_{dq} is greater than V_c . And lower cutting speed and feed rate can achieve lower surface roughness, which means higher surface quality. Aslantas et al. (Ref 21) investigated the effect of milling parameters, including spindle speed n (5000-60,000 rev/min), f_z (0.1-30 $\mu\text{m/tooth}$), and axial depth of cut a_p (5-250 μm), on the machined surface roughness (S_a and S_z), and performed milling on Ti-6Al-4V alloy using end mills. The results show that the surface roughness first decreases and then increases with the increase of n and f_z , and reaches the minimum value (about $0.22 \mu\text{m}$) at $n = 15,000 \text{ rev/min}$ and $f_z = 2 \mu\text{m/tooth}$, respectively. Besides, the surface roughness always increases with the increase of axial depth of cut a_p .

As a quantitative description method based on statistics, all surface roughness parameters vary with the observation scale (Ref 22) and are usually limited by the sampling length (Ref 23, 24). Therefore, there will be some deviations in the random characteristics and some local defect details of the machined surface topography (Ref 25). And traditional statistical parameters cannot accurately express the real characteristics of the machined surface (Ref 26, 27). In general, surface defects induced in peripheral milling vary from nano- to macroscales,

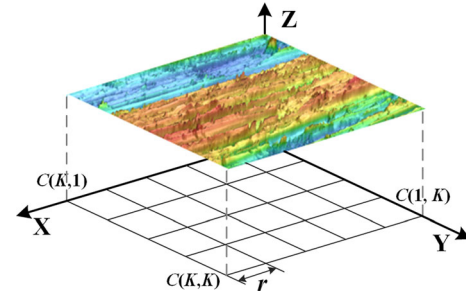
Table 1 Physical/functional significance of several surface roughness parameters

Functional properties	R_a, R_q	R_p, R_{pm}	R_z, R_z	R_{sk}	R_{ku}	R_{sm}	W_a
Contact stiffness	*		*	*	*	*	*
Fatigue strength	*	*	*		*		
Thermal conductivity	*	*				*	*
Electrical conductivity	*					*	*
Reflexivity			*				
Friction and wear	*		*	*	*	*	*
Lubrication	*	*	*	*	*		*
Mechanical sealing	*		*	*			*
Fatigue corrosion	*	*		*		*	
Assembly tolerances	*		*				*

which causes microstructural, mechanical, and chemical effects (Ref 28). In particular, the small-scale surface topography may be extremely important for predicting and tailoring surface characteristics such as adhesion, friction, and wear (Ref 29). However, surface topography will often appear to be different when observed at different scales (Ref 30). A surface that is rougher at a larger scale may be smoother at a smaller scale and vice versa (Ref 29). Therefore, a multi-scale analysis of the machined surface is required (Ref 30, 31).

Actually, the machined surface consists of a series of random microtopography features that show continuity, non-differentiable, and self-affinity in mathematics (Ref 32-34). Fractal theory is a newly developing subject of nonlinear problems, which is an effective tool for analyzing irregular things and phenomena with self-similar structures. The fractal dimension obtained by fractal theory is a multi-scale characterization parameter independent of the measured size (Ref 24), which can reflect the irregularity and fragmentation of the surface (Ref 35, 36). Mao et al. (Ref 23) evaluated end-milling surface quality of 2A12 aluminum alloy based on surface profile (Two-dimensional or 2D) fractal dimension and surface roughness R_q . Further research has shown that fractal analysis is more effective at meso-scale than surface roughness R_a , especially for features whose sizes are small or even smaller than the sampling length. Qu et al. (Ref 27) carried out roughness characterization (S_a and S_q) and fractal characterization on the milling surface of Elgiloy and found that fractal dimension can reflect some features of the surface that roughness parameters cannot, because surfaces with similar roughness have different fractal dimensions. Karolczak et al. (Ref 37) used fractal theory and roughness parameters (S_a, S_z, S_{sk} , and S_{ku}) to evaluate the surface of aluminum composites after tuning. The results show that the spatial (three-dimensional or 3D) fractal dimension can be treated as a tool to describe the irregularity of the machined surface. Because it has values above 2.6 for machined surfaces where numerous irregular adhering particles or built-up edges were observed. Wang et al. (Ref 38) chose S_a, S_q , and 3D fractal dimension to evaluate the milling surface of Ti-6Al-4V alloy under different milling parameters and found that 3D fractal dimension represents the complexity of details on the surface. Moreover, the fractal dimension is more sensitive to surface defects than roughness parameters. Although many studies have been conducted on the fractal analysis of machined surfaces, the multi-scale surface fractal characteristics of Ti-6Al-4V in peripheral milling have not been explored.

In the present study, peripheral milling-induced surface topography is evaluated by statistical and fractal analysis

**Fig. 1** Surface division diagram in the RSE method

methods at different scales. Firstly, the macro- and microdefects characteristics of the machined surface and their formation mechanisms are clarified. And then, the response laws of profile, height, and spatial surface roughness with peripheral milling parameters at different scales are revealed through the combination of surface topography analysis. Finally, the fractal dimension calculation method of the machined surface is given, and the multi-scale fractal characteristics of the peripheral milling-induced surface with milling parameters are explored.

2. Surface Characterization Method

2.1 Surface Roughness

Surface topography has a significant impact on the performance of component, such as contact stiffness, fatigue strength, and thermal conductivity. According to the physical/functional significance corresponding to different roughness parameters (Ref 39), as shown in Table 1, and considering that Ti-6Al-4V alloy parts are commonly used in a complex environment with high temperature, severe corrosion and high assembly accuracy requirements, etc., 2D profile, height and spatial parameters including arithmetical mean deviation R_a , maximum height R_z , kurtosis R_{ku} and skewness R_{sk} defined in ISO 4287 (Ref 40) are selected in this study, as well as their corresponding 3D roughness S_a, S_z, S_{ku} , and S_{sk} defined in ISO 25178-2 (Ref 41).

2.2 Fractal Characterization

Fractal geometry was originally used to describe the irregular geometry. It has been proved that most surfaces obey the fractal self-affine symmetry (Ref 42), and machined surfaces are no exception. There are several traditional methods

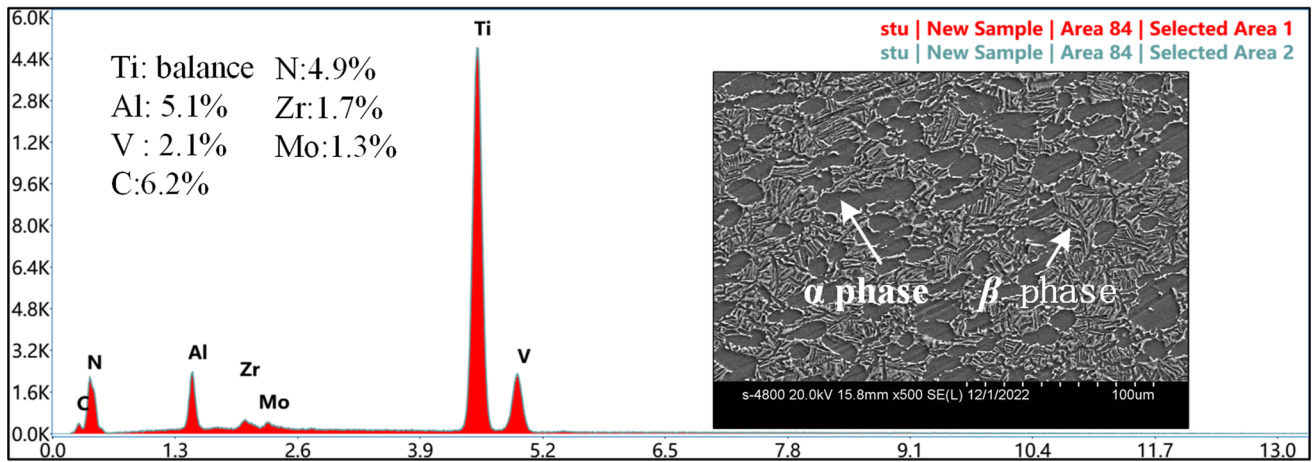


Fig. 2 Energy spectrum analysis and microstructure of Ti-6Al-4V alloy

Table 2 Thermo-mechanical properties of Ti-6Al-4V

Density, cm ³	g/	Elastic modulus, GPa	Yield strength, MPa	Tensile strength, MPa	Thermal conductivity, W/m·K	Specific heat, J/(Kg·K)
4.43		110	931	1014	7.3	709

Table 3 Peripheral milling parameters of Ti-6Al-4V alloy

Experiment No.	Spindle speed n , rev/min	Radial depth of cut a_e , mm	Feed rate f , mm/rev
T1	400	0.2	0.06
T2	400	0.3	0.10
T3	400	0.4	0.14
T4	400	0.5	0.18
T5	650	0.2	0.10
T6	650	0.3	0.06
T7	650	0.4	0.18
T8	650	0.5	0.14
T9	900	0.2	0.14
T10	900	0.3	0.18
T11	900	0.4	0.06
T12	900	0.5	0.10
T13	1150	0.2	0.18
T14	1150	0.3	0.14
T15	1150	0.4	0.10
T16	1150	0.5	0.06

to calculate the fractal dimension D , such as box counting method (Ref 43), variation method (Ref 44), and roughness scaling extraction method (Ref 45). Among the existing methods, due to the advantages of simple calculation, high accuracy, explicit physical meaning, and flexible surface adaptability (Ref 45-47), the roughness scaling extraction (RSE) method is used for fractal analysis in the present study. And the fractal dimension is calculated based on the RSE method using MATLAB software.

In the RSE method, the projection area of the 3D surface on the XOY plane is divided into $K \times K$ square cells with the side length of r , as shown in Fig. 1.

In this method, the side length r of the grid is used as the measurement scale. On the one hand, it is necessary to ensure

that the machined surface is fully covered, while on the other hand, avoiding missing any detailed information on the machined surface. Therefore, the side length r was set to be 1-6 times longer than the minimum resolution under different observation scales in this paper. The cell of row i and column j is defined as $C(i, j)$, where $C(i, j) = \{(x, y) | (i-1)r \leq x < ir, (j-1)r \leq y < jr\}$, and $i, j = \{1, 2, \dots, K\}$. And the root-mean-square $R_{i,j}(r)$ at $C(i, j)$ is given by

$$R_{i,j}(r) = \sqrt{E\{[z(x, y) - E\{z(x, y)\}]^2\}} \quad (\text{Eq 1})$$

where $z(x, y)$ is the height value at point (x, y) and $E\{\dots\}$ means the mean value. The relationship between the root-mean-

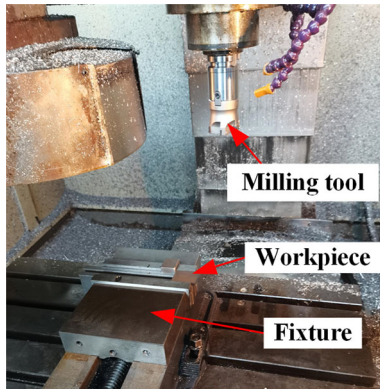


Fig. 3 Experimental machine tool

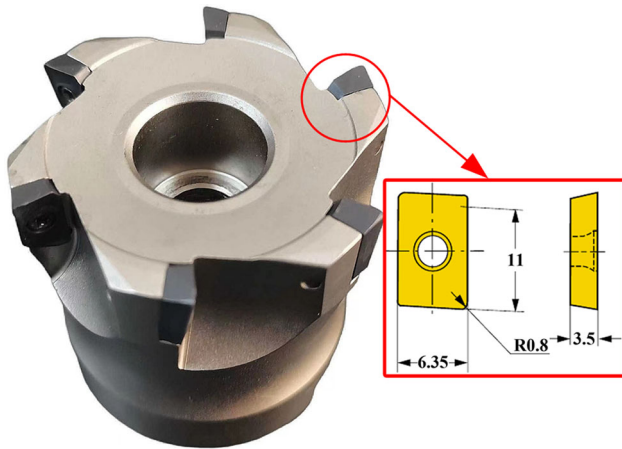


Fig. 4 Milling tool and blade (mm)

square $R(r)$ of the whole surface and the grid side length r is shown in Eq 2.

$$R(r) = E\{R_{ij}(r)\} \sim r^{3-D} \quad (\text{Eq } 2)$$

3. Experiment Setup

3.1 Workpiece Material

The material Ti-6Al-4V used for experiments is a $\alpha + \beta$ two-phase titanium alloy, which is produced by forging. The initial energy spectrum and microstructure of Ti-6Al-4V alloy are shown in Fig. 2. And the thermo-mechanical properties parameters of Ti-6Al-4V are shown in Table 2 (Ref 21), respectively. The workpiece dimensions are 40 mm \times 30 mm \times 5 mm.

3.2 Milling Conditions

As a multi-factor and multi-level experimental design method, the Taguchi method is used in this study. It can not only solve the problem of multi-factor optimization, but also analyze the impact of various factors on the test results, so as to capture the main factors. Before designing the experiment, the main peripheral milling parameters that affect the machining of Ti-6Al-4V alloy are selected: spindle speed n , feed rate f , and

radial depth of cut a_e . And the axial depth of cut a_p is set to the same value as the height of Ti-6Al-4V workpiece to ignore its influence. A three-factor and four-level Taguchi orthogonal experiment $L_{16}(4^3)$ was designed, and the peripheral milling parameters are shown in Table 3.

Milling experiments were carried out on the CNC machining center (GJ SEIKO LM-6050), as shown in Fig. 3. A right-angle six-tooth milling tool with a diameter of 50 mm was used, as shown in Fig. 4. The milling mode was down milling. The carbide AlTiN (PVD) coated indexable cutter blade (APPT1135PESR-FS KC522M) produced by Kennametal Company was adopted in the experiment, which has an effective cutting length of 11 mm. The KC522M material has better performance in the superalloy processing, which not only prevents the cutter blade from breaking, but also has better wear resistance and strength (Ref 48). For the sake of safety and environmental protection, dry milling was adopted. In addition, each group of experiments was conducted twice in order to avoid the influence of random errors.

3.3 Measurement of Surface Topography

After milling, the 3D digital images of the machined surface topography were measured at different scales by using a 3D laser scanning confocal microscope (VK-X260K, KEYENCE). In order to observe surface topography at different macro- and microscales, magnifications were set at 200 \times , 400 \times and 1000 \times to characterize the surface features according to the equipment parameters. The sizes of the detection area were approximately 1.07 \times 1.43, 0.53 \times 0.71, and 0.21 \times 0.29 mm², with resolutions of 1.39, 0.70, and 0.28 μ m, respectively. After the measurement, a Gaussian filter based on the Fourier transform was used to separate surface waviness and surface roughness with a cutoff length of 0.8 mm according to ISO 25178-3 (Ref 49). In addition, the surface roughness was measured with the evaluation length of 1.43, 0.71, and 0.29 mm, respectively. In the process of measurement, three areas were selected on the machined surface of the workpiece along the feed direction for 3D surface topography evaluation in order to reduce the influence of random error, and the interval between the adjacent regions was set to about 1-2 mm.

In addition, the high-resolution scanning electron microscope (Regulus 8230, HITACHI) was used for energy spectrum analysis of surface defects after peripheral milling to determine their source.

4. Result and Discussion

4.1 Surface Defects

The milling surface topography measurement results of some samples at different observation scales are shown in Fig. 5.

Evenly distributed edges can be seen on the peripheral milling surface, as shown in Fig. 5(a) and (b), which are the feed marks generated by the relative motion between the milling tool and the workpiece, clearly reflecting the trajectory of the milling tool. The distance between two adjacent feed marks is affected by the feed rate. Due to the influence of the milling tool clearance angle, scratches along the feed direction are observed clearly between adjacent feed marks.

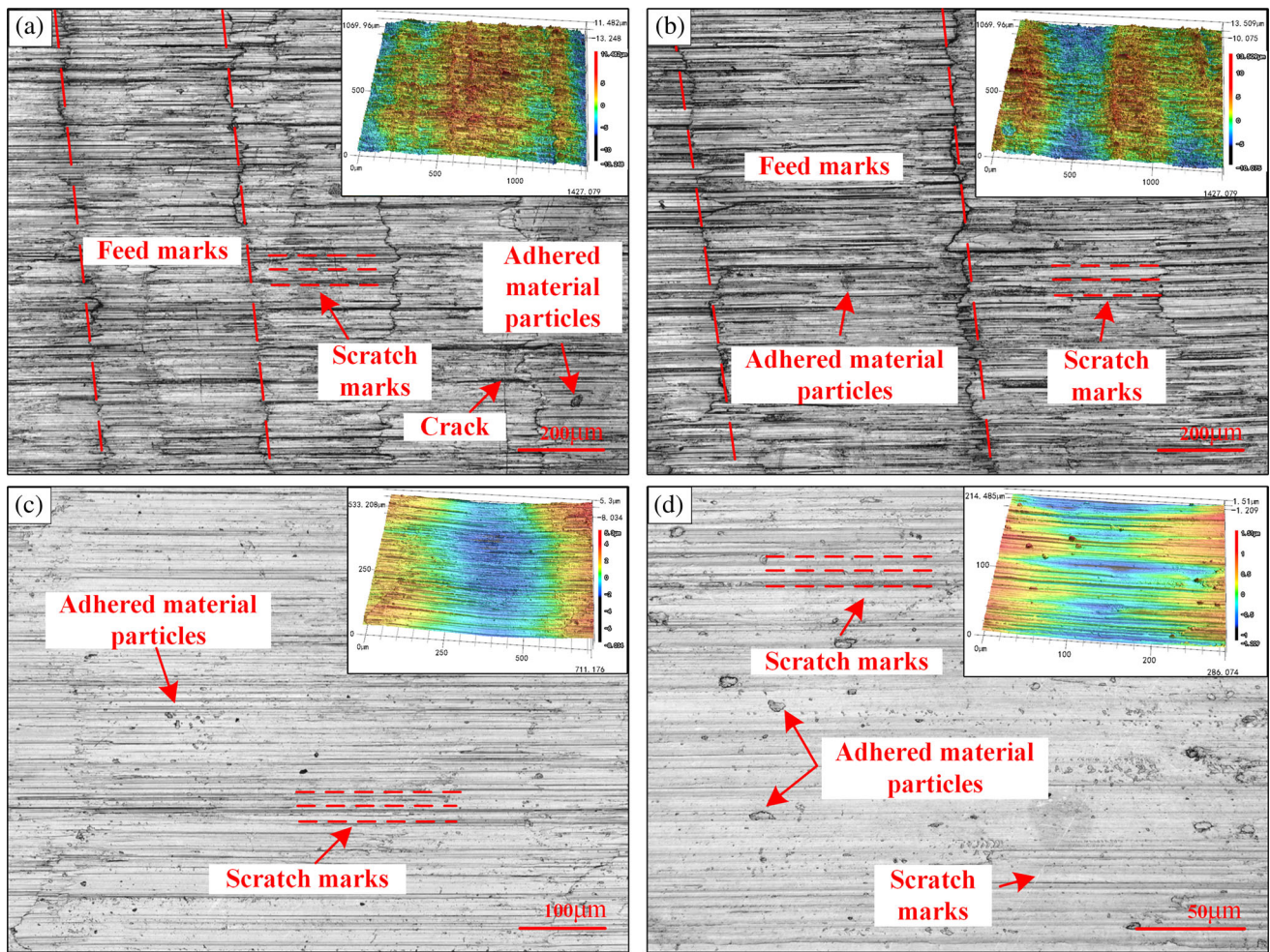


Fig. 5 Surface topography under different milling parameters and scales: (a) T2 at 200 × ; (b) T7 at 200 × ; (c) T9 at 400 × ; (d) T15 at 1000 ×

Randomly adhered material particles are also observed on the peripheral milling surface, Fig. 5(c) and (d), which may be microchips, hard particles peeling off from the tool, etc. (Ref 50). The energy spectrum detection is performed on the adhered material particles on the milling surface, as shown in Fig. 6(a), which is substantially the same as the titanium alloy (Ti-6Al-4V) matrix material. It can be inferred that adhered material particles are mainly formed by welding high-temperature microchips to the surface during peripheral milling. There are also some randomly unoriented scratches, which may be caused by hard particles peeling off from the milling tool, built-up edges, and other hard points rolling on the surface (Ref 51, 52). As shown in Fig. 6(b), the energy spectrum analysis result of the scratch is basically the same as the Ti-6Al-4V alloy matrix material. It can be inferred that the formation of randomly unoriented scratches can be attributed to the built-up edges or chips sliding between the tool and the milling surface. In addition, cracks are present in the surface due to high levels of thermal and mechanical stress that exist in the machining zone in the case of dry milling (Ref 53).

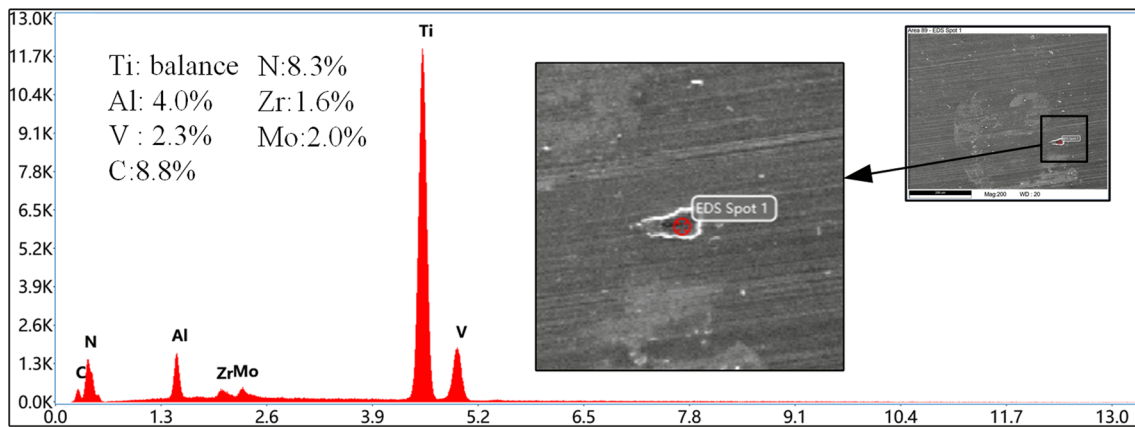
According to the formation mechanism and distribution features, surface defects of the Ti-6Al-4V alloy in peripheral milling can be categorized into two types: natural defects and random defects, where feed marks and scratches along the feed

direction are natural defects, adhered material particles, random scratches, and cracks are random defects.

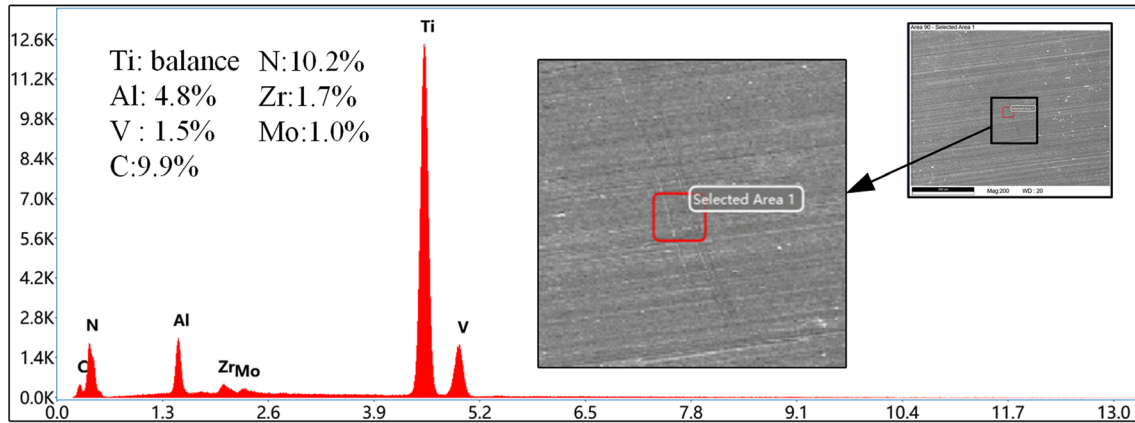
4.2 2D Surface Roughness

Table 4 and Fig. 7 show the influence of different milling parameters on the 2D roughness R_a and R_z of the machined surface along the feed direction. It can be seen from the figures that the values of R_a and R_z decrease gradually with the increase of observation scale. In addition, R_a and R_z exhibit almost similar trends with milling parameters at different scales, but the value of R_z has always been greater than R_a .

In Fig. 7(a), the values of R_a and R_z decrease almost linearly as the spindle speed n increases from 400 to 900 rev/min, where the percentage decreases of R_a and R_z are 24.04 and 17.76% at 200 ×, 41.09 and 36.72% at 400 ×, respectively, and reach the minimum value ($R_a = 0.944$ and $R_z = 6.775$ at 200 ×, $R_a = 0.376$ and $R_z = 2.203 \mu\text{m}$ at 400 ×) at $n = 900$ rev/min. With the spindle speed exceeding 900 rev/min, the surface roughness shows an increasing trend. However, the roughness R_a and R_z almost linearly decreases with the spindle speed increasing at the observation scale of 1000 ×, and the percentage decreases are 61.29 and 48.72%, respectively. This is because the milling surface topography at the scale of 1000 × is smoother compared to other scales, as



(a)



(b)

Fig. 6 Energy spectrum of defects on the peripheral milling surface: (a) adhered material particle; (b) small scratch

Table 4 R_a and R_z of machined surface at different milling parameter

Experiment No.	200 ×		400 ×		1000 ×	
	$R_a, \mu\text{m}$	$R_z, \mu\text{m}$	$R_a, \mu\text{m}$	$R_z, \mu\text{m}$	$R_a, \mu\text{m}$	$R_z, \mu\text{m}$
T1	1.132	7.886	0.410	2.805	0.352	1.553
T2	1.262	8.389	0.702	3.689	0.382	1.683
T3	1.605	9.571	1.075	5.184	0.518	2.179
T4	0.969	7.108	0.364	2.246	0.246	1.207
T5	0.991	7.013	0.479	2.827	0.187	1.137
T6	1.033	7.096	0.393	2.462	0.320	1.603
T7	1.362	8.213	0.706	3.839	0.330	1.609
T8	1.049	7.166	0.440	2.585	0.281	1.284
T9	1.075	7.305	0.500	2.535	0.297	1.399
T10	0.929	7.123	0.305	2.047	0.161	0.905
T11	0.797	5.448	0.352	2.059	0.120	0.733
T12	0.974	7.225	0.346	2.171	0.180	0.956
T13	1.056	7.148	0.376	2.532	0.182	0.970
T14	0.949	6.985	0.341	2.399	0.135	0.757
T15	0.947	7.124	0.458	2.492	0.146	0.859
T16	0.937	7.072	0.353	2.262	0.118	0.809

shown in Fig. 5. The height fluctuation along the feed direction on the milling surface is more susceptible to the influence of surface defects such as adhered material particles and scratches.

Generally, the increase of spindle speed means the increase of material deformation rate, which leads to more heat

generation during the milling process. The accumulation of heat between the contact surface of the milling tool and the workpiece causes a thermal softening effect on the titanium alloy (Ti-6Al-4V) material, which makes it easier to cut off and results in a decrease in surface roughness (Ref 2, 54). However,

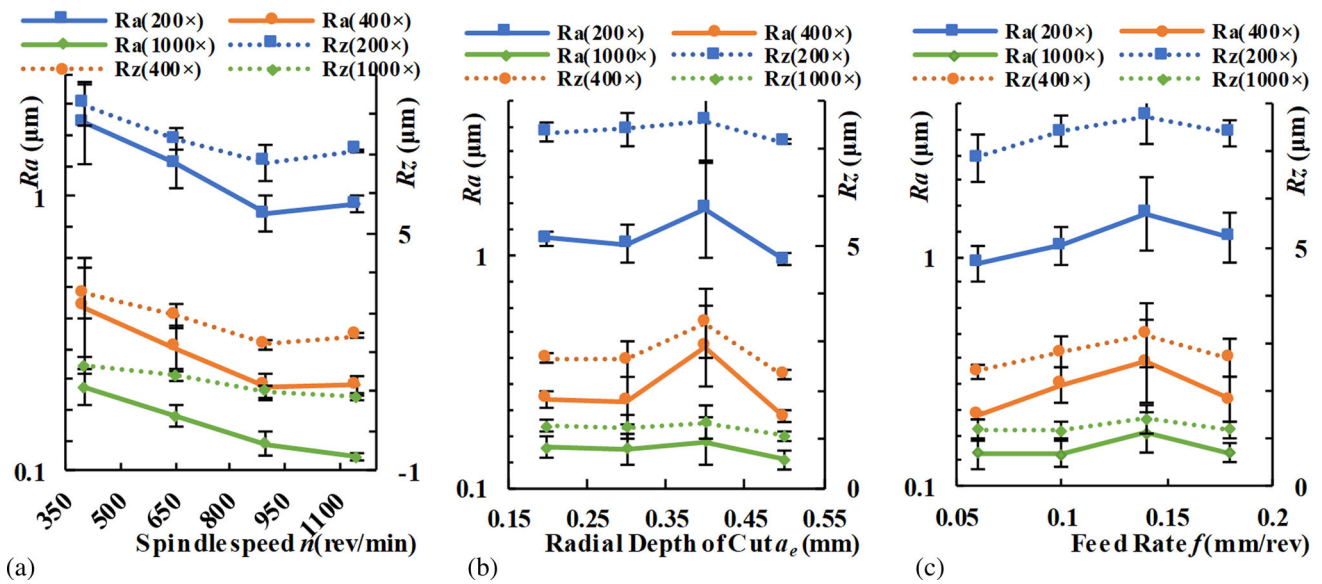


Fig. 7 Effect of milling parameters on roughness R_a and R_z at different scales. (a) Spindle speed n (b) Radial depth of cut a_e (c) Feed rate f

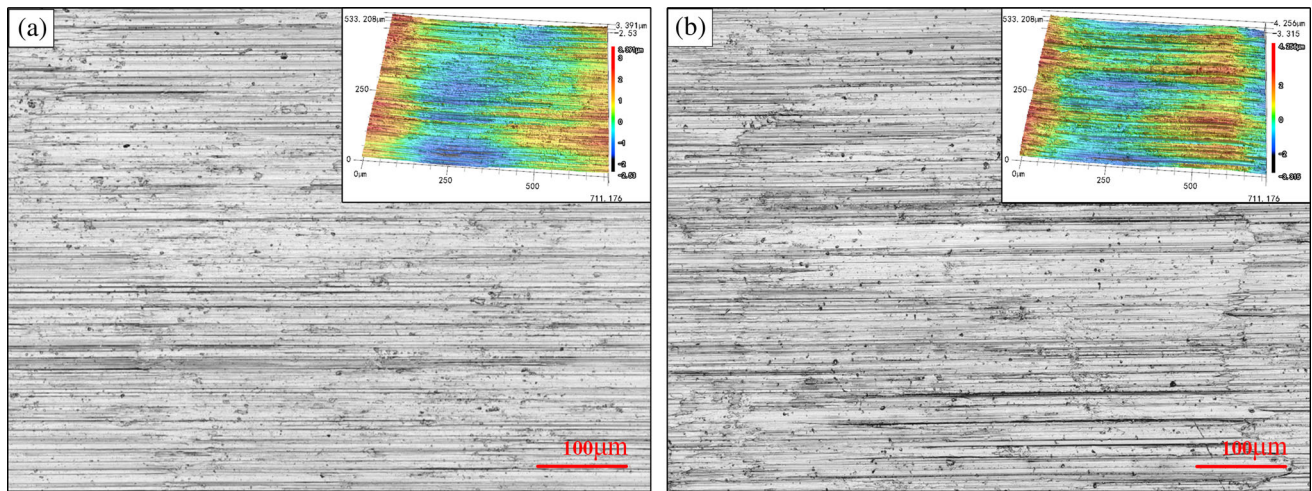


Fig. 8 Surface topography under different spindle speed n : (a) T11 at 400 \times ; (b) T16 at 400 \times

the accumulated heat on the contact surface will be difficult to dissipate quickly when the spindle speed continues to increase, leading to an expansion in the adhesion of chips to the milling tool and machined surface (Ref 55), thus increasing the milling force. Besides, the impact of strain and strain rate of reinforcement on the milling force is greater than thermal softening at a higher spindle speed, which also causes a rising trend in the milling force (Ref 56-58). According to the regenerative chatter theory, if the milling force exceeds and extends where the stiffness of milling system is too weak to maintain the stable vibration, a chatter will happen (Ref 12, 59), thereby deteriorating the milling surface and resulting in an increase in surface roughness. As shown in Fig. 8(a) and (b), the surface quality deteriorates as the spindle speed increases from 900 to 1150 rev/min. The surface height fluctuation obtained at $n = 1150$ rev/min is much greater than that obtained at $n = 900$ rev/min, and the number of adhered material particles on the surface is more than that at $n = 900$ rev/min according to the height cloud map in the upper right corner.

In Fig. 7(b), the values of surface roughness R_a decrease slightly and then increase significantly as the radial depth of cut a_e increases from 0.2 to 0.4 mm, and the maximum percentage decrease is only 1.91%. On the one hand, the workpiece is pre-processed before machining to find a flat surface. The extrusion and friction between the flank surface of the milling tool and the surface of the workpiece can result in fibrosis, which contributes to hardening the surface to be machined (Ref 60, 61). On the other hand, the chemical activity of titanium alloys Ti-6Al-4V is very high and it is easy to react with elements in the air, producing a surface hardening layer (Ref 62, 63), which also leads to an increase in surface hardness. Therefore, the milling tool can avoid the surface hardening layer to a certain extent and cut the material more easily by appropriately increasing the radial depth of cut, which slightly reduce the surface roughness. As shown in Fig. 9(a) and (b), the number of adhered particles and scratches on the surface decreases as the radial depth of cut increases from 0.2 to 0.3 mm, and the change in surface height along feed direction becomes smoother. However, the cross-sectional area of the material

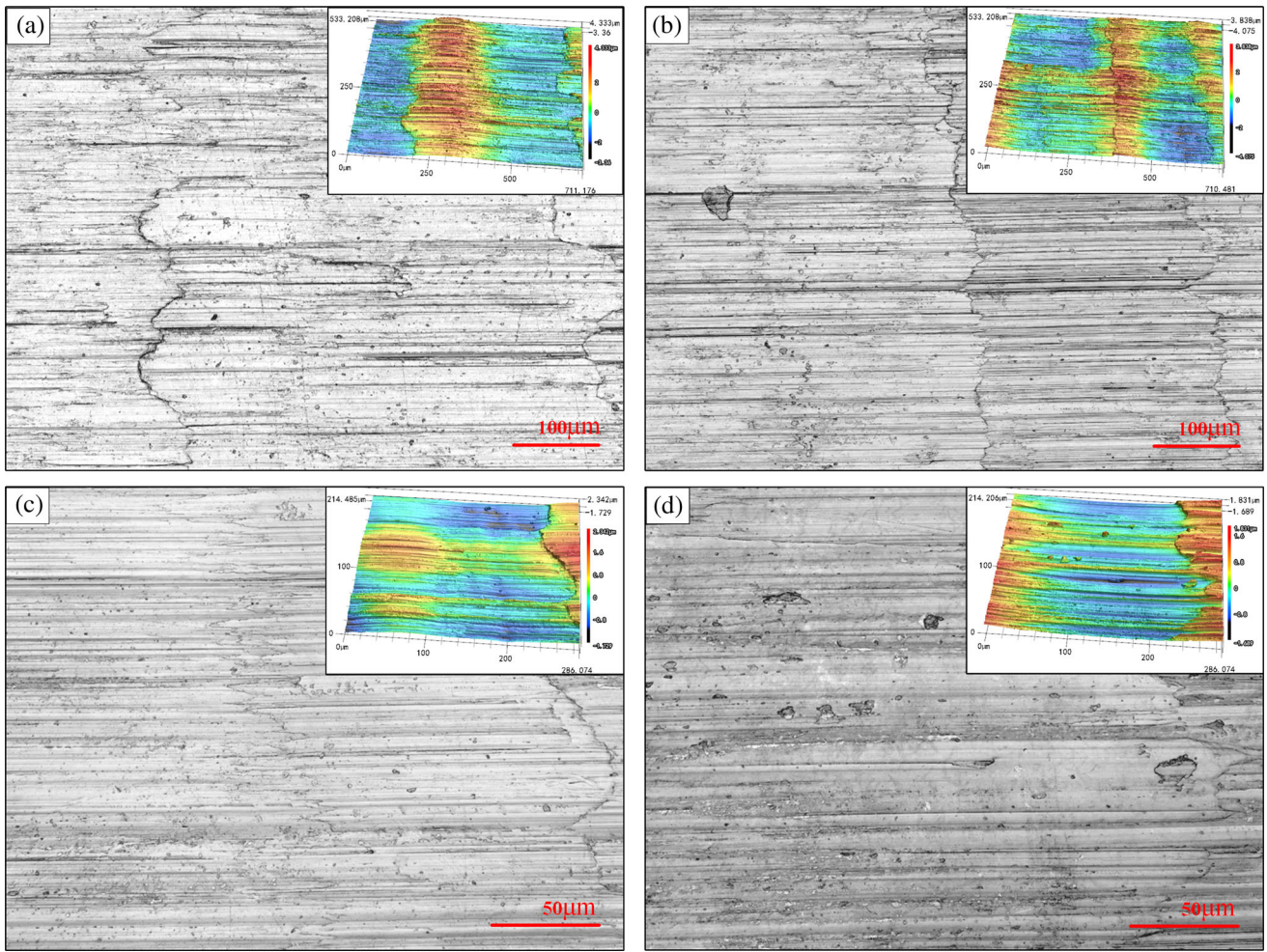


Fig. 9 Surface topography under different radial depth of cut a_r : (a) T5 at 400 ×; (b) T6 at 400 ×; (c) T6 at 1000 ×; (d) T7 at 1000 ×

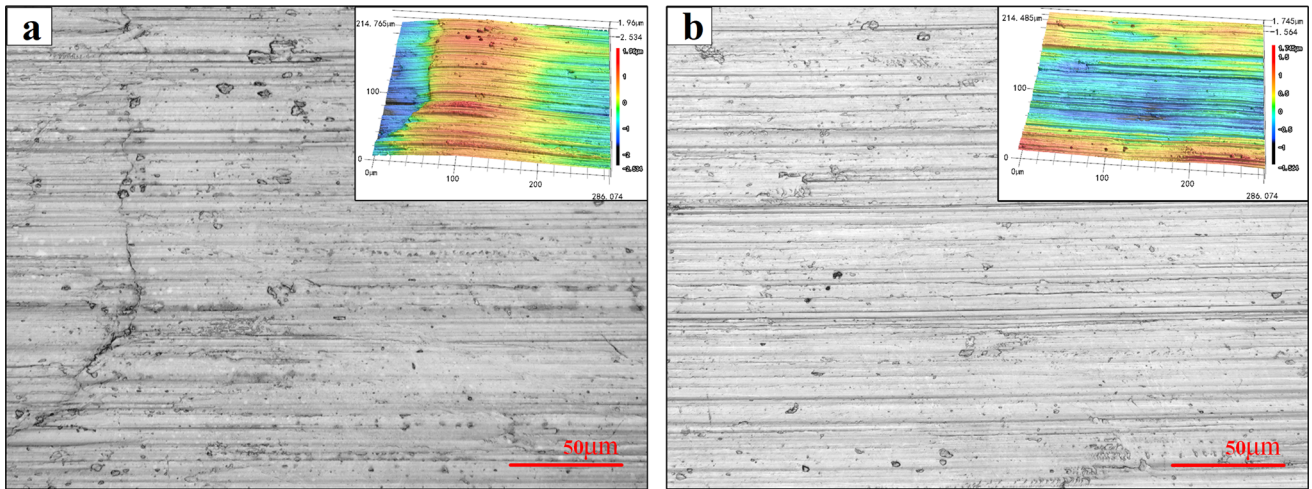


Fig. 10 Surface topography under different feed rate f : (a) T9 at 1000 ×; (b) T13 at 1000 ×

shear zone increases as the radial depth of cut increases, which means that the contact area and contact time between the tool and the workpiece also increase accordingly. And the increase in material removal rate per unit time will lead to an increase in milling force, which makes the tool more prone to vibration and reflected on the machining surface. Eventually, the surface

roughness increases. As shown in Fig. 9(c) and (d), the increase of the radial depth of cut results in an increase of randomly distributed adhered particles on the surface and deterioration of surface quality. Then, the surface roughness shows a decreasing trend when the radial depth of cut exceeds 0.4 mm. This is because the further increase of extrusion deformation makes the

Table 5 R_{sk} and R_{ku} of machined surface at different milling parameter

Milling parameters	200 ×		400 ×		1000 ×	
	R_{sk}	R_{ku}	R_{sk}	R_{ku}	R_{sk}	R_{ku}
Spindle speed n , rev/min						
400	0.352	2.984	0.507	2.745	0.221	2.720
650	0.185	2.974	0.608	2.829	0.274	2.802
900	0.269	3.199	− 0.040	2.745	0.085	2.775
1150	0.137	3.197	− 0.073	2.777	0.230	3.345
Radial depth of cut a_e , mm						
0.2	0.097	2.981	0.163	2.895	0.281	2.738
0.3	0.414	3.210	0.379	2.872	0.152	2.816
0.4	0.246	2.883	0.254	2.526	0.205	2.711
0.5	0.186	3.280	0.205	2.803	0.171	2.777
Feed rate f , mm/rev						
0.06	0.297	3.128	0.313	2.946	0.286	3.012
0.10	0.445	3.264	0.364	2.665	0.162	2.811
0.14	0.228	2.972	0.087	2.644	0.074	2.476
0.18	− 0.027	2.990	0.237	2.842	0.288	2.743

Table 6 S_a and S_z of machined surface at different milling parameter

Experiment No.	200 ×		400 ×		1000 ×	
	S_a , μm	S_z , μm	S_a , μm	S_z , μm	S_a , μm	S_z , μm
T1	1.400	17.694	0.682	9.228	0.661	4.314
T2	1.520	17.818	0.851	7.976	0.580	4.174
T3	1.728	19.540	1.115	10.546	0.573	3.985
T4	1.355	21.761	0.549	7.302	0.349	3.129
T5	1.246	15.655	0.638	5.934	0.325	3.044
T6	1.177	15.659	0.555	5.901	0.489	3.818
T7	1.492	17.976	0.790	8.238	0.399	3.503
T8	1.309	17.464	0.545	8.327	0.356	3.601
T9	1.258	24.028	0.598	7.794	0.339	3.403
T10	1.362	15.809	0.475	6.718	0.259	2.408
T11	1.085	15.149	0.471	5.660	0.231	2.285
T12	1.296	16.113	0.471	5.637	0.257	2.426
T13	1.417	17.701	0.535	6.888	0.317	2.884
T14	1.304	14.373	0.527	6.335	0.283	2.668
T15	1.348	17.927	0.577	9.737	0.248	2.659
T16	1.401	22.825	0.580	9.011	0.475	3.662

milling temperature rise, and the surface thermal softening effect becomes significant. Therefore, the surface material is easier to remove and the surface quality is improved.

It can also be seen from Fig. 7(b) that there are some differences between the variation trend of R_z and R_a . The roughness R_z increases continuously with the increase of radial depth of cut a_e from 0.2 to 0.4 mm and does not show a slight downward trend at 200 ×. This is because the roughness R_z is particularly susceptible to surface defects in the feed direction, especially adhered material particles of different sizes.

In Fig. 7(c), the values of surface roughness R_a and R_z increase with the feed rate f increasing from 0.06 to 0.14 mm/rev. The percentage increases of R_a are 19.9% at 200 ×, 56.3% at 400 ×, and 35.3% at 1000 ×, respectively. And the percentage increases of R_z are 12.8% at 200 ×, 32.5% at 400 ×, and 19.6% at 1000 ×, respectively. Then, surface

roughness R_a and R_z show a decreasing trend as the feed rate f exceeds 0.14 mm/rev.

The spacing and morphological differences between adjacent peaks and valleys on the machining surface increase when the feed rate increases from 0.06 to 0.14 mm/rev, due to the reduction in cutting times per unit cutting area by the milling tool in the feed direction. And the residual height of the milling tool on the machined surface increases, ultimately leading to an increase in surface roughness. The percentage increase is between 12.82 and 56.29%. Especially in Fig. 5(a) and (b), the uneven spacing of feed marks deteriorates surface quality, which can be attributed to the increase in milling force causing the milling tool to vibrate during the machining process (Ref 64). However, as the feed rate increases further, the milling temperature will have a softening effect on the surface of titanium alloy Ti-6Al-4V, which lead to simpler material removal and a decrease in surface roughness. Another possible

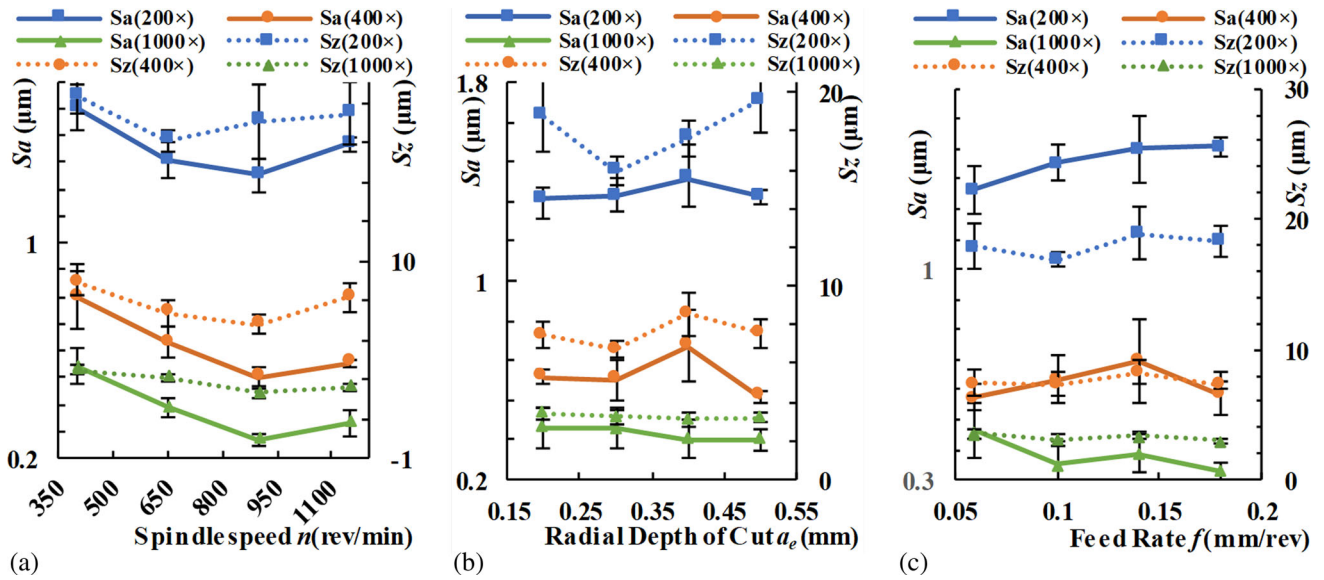


Fig. 11 Effect of milling parameters on roughness S_a and S_z at different scales. (a) Spindle speed n (b) Radial depth of cut a_e (c) Feed rate f

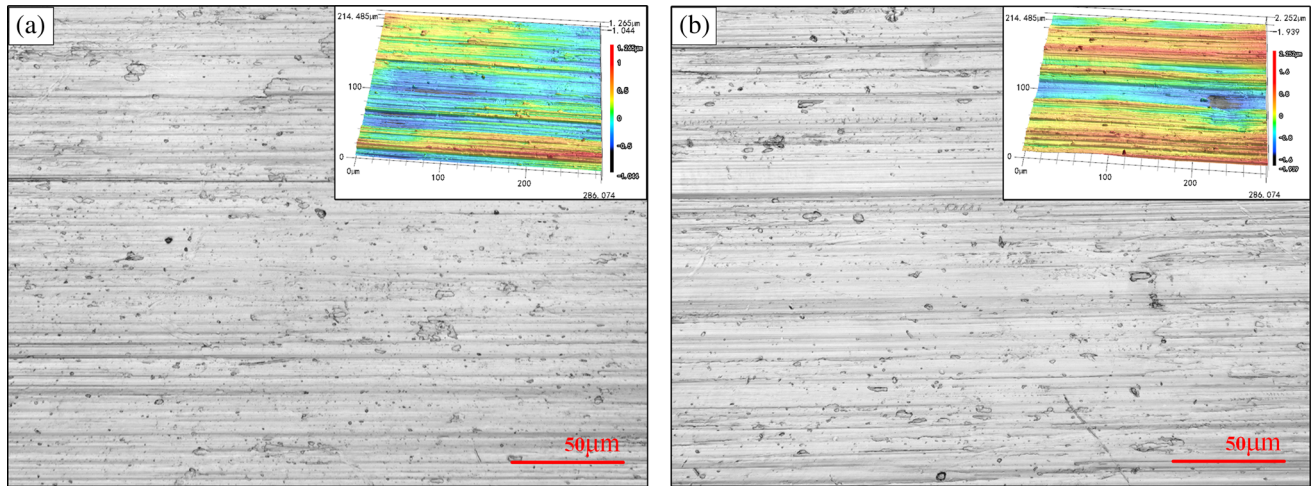


Fig. 12 Surface topography under different spindle speed n : (a) T11 at 1000 \times ; (b) T16 at 1000 \times

explanation is given by smearing effects (Ref 65). During the milling process, the high-temperature workpiece material is extruded by the tool and smeared onto the machined surface, which could reduce the roughness peaks of the workpiece material resulting in a lower surface roughness value. This phenomenon is promoted by higher mechanical and thermal loads due to ploughing and thermal softening. As shown in Fig. 10(a) and (b), when the feed rate increases from 0.14 to 0.18 mm/rev, the number of grooves, adhered particles and protrusions on the milling surface decreases, and the scratches become clearer and more uniform, indicating that the surface quality has improved.

In order to obtain the specific value of the contribution rate of each factor, the analysis of variance (ANOVA) is conducted. At the observation of 200 \times , the significance contribution of milling parameters for R_a and R_z are spindle speed (46.91%) > radial depth of cut (16.67%) > feed rate (16.05%) and spindle speed (52.74%) > feed rate (17.70%) > radial depth of cut (4.48%), respectively. At 400 \times , the significance contribution of milling parameters for

R_a and R_z are spindle speed (34.86%) > radial depth of cut (32.57%) > feed rate (18.86%) and spindle speed (43.72%) > radial depth of cut (27.75%) > feed rate (14.11%), respectively. And at 1000 \times , the significance contribution of milling parameters for R_a and R_z are spindle speed (69.49%) > feed rate (11.86%) > radial depth of cut (6.78%) and spindle speed (72.43%) > radial depth of cut (7.40%) > feed rate (7.39%), respectively. It can be seen that the spindle speed has the greatest impact on the roughness R_a and R_z at different observation scales.

Table 5 shows the effect of milling parameters on the surface skewness R_{sk} and kurtosis R_{ku} . It can be seen that the values of R_{sk} are basically positive, which indicates that the height distribution along the feed direction is lower than the mean plane and there are some peaks on the surface, especially the feed marks. Some surface skewness is negative but very close to 0, such as $R_{sk} = -0.040$ ($n = 900$ rev/min, 400 \times), which may be caused by some scratches and dents on the surface. The parameter R_{ku} characterizes the spread of the height distribution. It can be seen from the table that the values of R_{ku}

Table 7 S_{sk} and S_{ku} of machined surface at different milling parameter

Milling parameters	200 ×		400 ×		1000 ×	
	S_{sk}	S_{ku}	S_{sk}	S_{ku}	S_{sk}	S_{ku}
Spindle speed n (rev/min)						
400	0.380	3.154	0.291	2.900	0.169	2.625
650	0.302	3.087	0.191	2.831	0.097	2.794
900	0.451	3.247	0.261	2.980	0.092	3.032
1150	0.453	3.265	0.076	3.032	− 0.053	2.834
Radial depth of cut a_e (mm)						
0.2	0.364	3.159	0.196	2.971	0.195	2.890
0.3	0.377	3.126	0.251	2.910	− 0.005	2.726
0.4	0.367	3.123	0.213	2.702	0.090	2.871
0.5	0.477	3.346	0.160	3.161	0.025	2.798
Feed rate f (mm/r)						
0.06	0.398	3.299	0.161	3.139	0.123	2.615
0.10	0.413	3.209	0.224	2.823	− 0.016	2.916
0.14	0.374	3.090	0.189	2.795	0.042	2.819
0.18	0.400	3.156	0.246	2.985	0.157	2.935

basically fluctuate around 3, indicating that the height distribution along the feed direction on the machined surface is smooth, without extreme peaks and valleys. It can be seen that the peripheral milling surface of Ti-6Al-4V alloy has good contact stiffness, fatigue strength, etc., as shown in Table 1.

4.3 3D Surface Roughness

Table 6 and Fig. 11 show the influence of different milling parameters on 3D surface roughness S_a and S_z . It can be seen that the values of S_a and S_z are slightly higher than those of R_a and R_z along the feed direction. And the values of 3D surface roughness also gradually decrease with the increase of the observation scale. Unlike the 2D roughness R_z , the variation trend of S_z is different from S_a but relatively chaotic at different observation scales. Especially at 1000 ×, S_z hardly changes with the change of milling parameters. This is due to 3D measurement since there are single peaks or valleys changing the value of S_z (Ref 37).

In Fig. 11(a), the values of surface roughness S_a have the same tendency of decreasing first and then increasing at different scales, reaching the minimum value at $n = 900$ rev/min. Especially at 1000 ×, the surface roughness S_a shows a rising trend as the spindle speed n exceeds 900 rev/min, which is opposite to 2D roughness R_a and R_q . As shown in Fig. 12, the increase in spindle speed reduces the defects along the feed direction on the milling surface at 1000 ×, which leads to a decrease in 2D roughness. However, the height fluctuation of defects such as scratches perpendicular to the feed direction is greater, resulting in an increase in 3D roughness.

In Fig. 11(b), the roughness S_a at 1000 × shows a decreasing trend when the radial cutting depth exceeds 0.3 mm, which is different from the change trend under other observation scales. In Fig. 11(c), S_a at 200 × increases continuously with the feed rate f increasing from 0.06 to 0.18 mm/rev. And the value of S_a at 400 × shows a decreasing trend when the feed rate f exceeds 0.14 mm/rev. However, S_a shows a fluctuating downward trend with the increase of feed rate at the observation scale of 1000 ×.

The analysis of variance (ANOVA) is performed to obtain the specific value of the contribution rate. At the observation of

Table 8 Fractal dimension D of machined surface at different milling parameter

Experiment No.	200 ×	400 ×	1000 ×
T1	2.7345	2.6555	2.4100
T2	2.7349	2.6484	2.4286
T3	2.7023	2.6409	2.4192
T4	2.6784	2.6061	2.3861
T5	2.7157	2.6557	2.4211
T6	2.7340	2.7033	2.4689
T7	2.7299	2.6641	2.4279
T8	2.7377	2.6831	2.4352
T9	2.7403	2.6902	2.4388
T10	2.7475	2.7024	2.4698
T11	2.7382	2.6949	2.4508
T12	2.7302	2.6706	2.4480
T13	2.7388	2.7005	2.4652
T14	2.7438	2.6942	2.4581
T15	2.7460	2.7004	2.4621
T16	2.7345	2.6936	2.4557

200 ×, the significance contribution of milling parameters for S_a and S_z are spindle speed (51.69%) > feed rate (19.10%) > radial depth of cut (6.74%) and radial depth of cut (35.31%) > spindle speed (15.47%) > feed rate (10.0%), respectively. At 400 ×, the significance contribution of milling parameters for S_a and S_z are spindle speed (53.17%) > radial depth of cut (22.22%) > feed rate (10.32%) and spindle speed (43.38%) > radial depth of cut (23.49%) > feed rate (8.75%), respectively. And at 1000 ×, the significance contribution of milling parameters for S_a and S_z are spindle speed (67.50%) > feed rate (17.50%) > radial depth of cut (3.75%) and spindle speed (67.42%) > feed rate (14.45%) > radial depth of cut (3.48%), respectively. It can also be seen that in most cases, the spindle speed has the greatest impact on the roughness S_a and S_z at different observation scales. However, the roughness S_z is most affected by the radial depth of cut, which can be attributed to the sensitivity of S_z to surface defects.

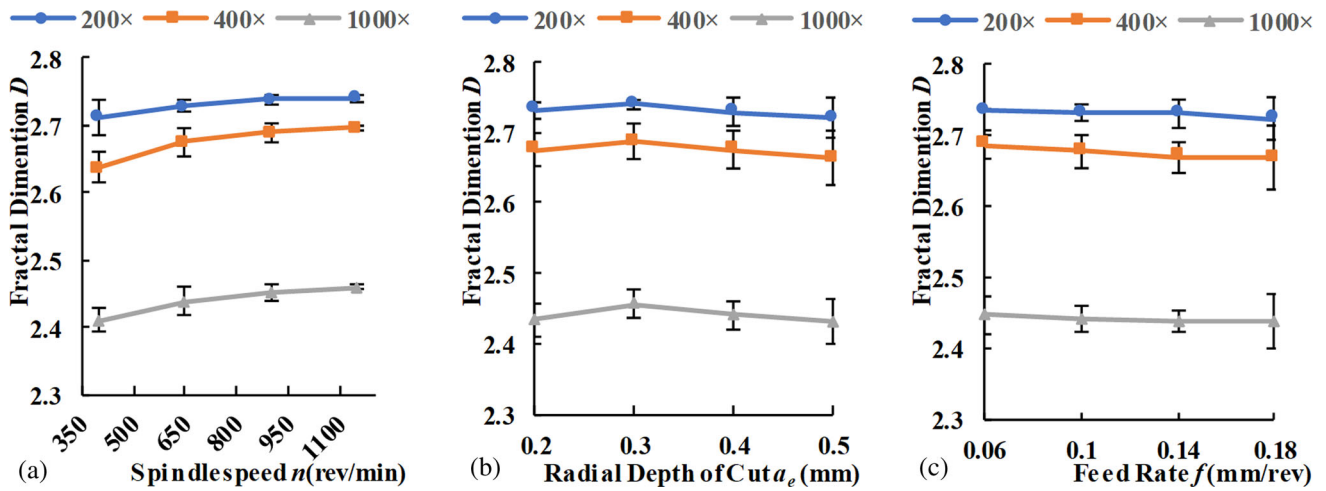


Fig. 13 Effect of milling parameters on fractal dimension D at different scales. (a) Spindle speed n (b) Radial depth of cut a_e (c) Feed rate f

Table 7 shows the effect of milling parameters on the surface skewness S_{sk} and kurtosis S_{ku} . It can be seen that S_{sk} is basically positive, indicating that there are relatively more peaks on the milling surface. However, there are some negative values of skewness S_{sk} at 1000 \times . Because the surface roughness obtained at a high observation scale is more susceptible to surface defects, and excessive scratches and pits can make the surface skewness negative. In addition, the values of S_{ku} are fluctuating around 3, indicating that the height distribution of the machined surface is smooth. Compared to R_{sk} and R_{ku} , S_{sk} and S_{ku} have an obvious feature of gradually decreasing with the observation scale increasing.

The difference in the trend of 3D and 2D surface roughness with the change of milling parameters, especially at the observation scale of 1000 \times , can be attributed to the fact that the milling surface of Ti-6Al-4V alloy includes not only surface features along the feed direction, but also features perpendicular to the feed direction, such as scratches and randomly adhered particles. In particular, the height fluctuation of scratches caused by the clearance angle of the milling tool cannot be ignored, which is perpendicular to the feed direction. On the Ti-6Al-4V milling surface as shown in Fig. 5, the height fluctuation of scratches perpendicular to the feed direction is much more severe than that in the feed direction, which cannot be characterized by the 2D roughness parameters along the feed direction. As the observation scale increases, scratches caused by the clearance angle and adhered particles become the main surface defects, and their impact on 3D surface roughness gradually increases. Therefore, the anisotropic microgeometry on the milling surface of Ti-6Al-4V alloy can be better represented by the 3D surface roughness, but it is insufficient at the observation scale of 1000 \times due to the effect of sampling length.

4.4 Fractal Analysis

Table 8 and Fig. 13 show the variation trend of the 3D fractal dimension D of the machined surface calculated by the RSE method under different milling parameters. The value of fractal dimension D represents the degree of irregularity, self-similarity and space filling on the surface. A larger fractal dimension D corresponds to more complex shapes and opulent microstructural details on the surface.

In Fig. 13(a), the 3D fractal dimension D increases with the increase of spindle speed n , but the increasing trend gradually decreases. The percentage increases of D are 1.04% at 200 \times , 2.25% at 400 \times , and 2.04% at 1000 \times , respectively. This means that the surface topography of Ti-6Al-4V in peripheral milling tends to become more complex with the increase of spindle speed. As shown in Fig. 8, when the spindle speed n increases from 900 to 1150 rev/min, the surface topography in peripheral milling tends to be complex, especially the scratches caused by the clearance angle of milling tool and randomly adhered particles make the greatest contribution.

In Fig. 13(b), the fractal dimension D increases first and then decreases almost linearly with the increase of radial depth of cut a_e . The fractal dimension D reaches the maximum value ($D_{max} = 2.740$ at 200 \times , $D_{max} = 2.687$ at 400 \times , and $D_{max} = 2.456$ at 1000 \times) when $a_e = 0.3$ mm, indicating that the complexity of machined surface obtained by $a_e = 0.3$ mm is the highest. As shown in Fig. 9(a) and (b), although the number of adhered material particles and random scratches on the milling surface decreases when the radial depth of cut a_e increases from 0.2 to 0.3 mm, the height variation of scratches caused by the tool clearance angle becomes more drastic perpendicular to the feed direction, which leads to an increase in the fractal dimension D of the overall peripheral milling surface.

In Fig. 13(c), the fractal dimension D of the milling surface decreases with the increase of feed rate f , but the value changes little. As the feed rate f increases from 0.06 to 0.18 mm/rev, the fractal dimension D decreases by 0.43% at 200 \times , 0.69% at 400 \times , and 0.37% at 1000 \times , respectively. It can be seen that the feed rate has the minimum effect on the 3D fractal dimension D . As shown in Fig. 10, an increase in feed rate f means less contact between the tool and the workpiece, the adhered material particles on the milling surface of Ti-6Al-4V alloy are reduced, and the height variation of scratches becomes more regular, thereby reducing the surface fractal dimension D .

The analysis of variance (ANOVA) is performed to obtain the specific value of the contribution rate. At the observation of 200 \times , the significance contribution of milling parameters for D is spindle speed (51.07%) > radial depth of cut (20.58%) > feed rate (7.24%). At 400 \times , the significance contribution of milling parameters for D is spindle speed (75.61%) > radial depth of cut (10.12%) > feed rate

(8.20%). And at $1000\times$, the significance contribution of milling parameters for D is spindle speed (70.62%) > radial depth of cut (19.33%) > feed rate (2.62%). It can be seen that the spindle speed has the greatest effect on fractal dimension D at different observation scales, while the feed speed has the smallest effect.

Combined with the surface topography mentioned in Fig. 5, it can be seen that the fractal characteristic of the surface topography of Ti-6Al-4V alloy in peripheral milling is influenced by a combination of many factors, including feed marks, randomly adhered particles, scratches caused by hard points or the clearance angle of the milling tool, intensity of surface height change, etc. The alteration of milling parameters produces diverse effects on the surface structure, and causes variations in the distribution and quantity of surface defects, which leads to a change of surface fractal dimension D . For example, an increase in the feed rate f can lead to an increase in the spacing between feed marks on the milling surface, which leads to a decrease in the fineness, complexity, and self-similarity of the surface structure, ultimately leading to a decrease in the fractal dimension of the machined surface.

It can also be seen that the value of surface fractal dimension D decreases with the increase of observation scale under the same milling parameter. The variation ranges of fractal dimension value are 2.713-2.741 at $200\times$, 2.638-2.697 at $400\times$, and 2.411-2.460 at $1000\times$, respectively. This is because the resolution and sampling length of the equipment change with the observation scale increasing, resulting in a decrease in the number of surface defects that can be obtained, especially the defects such as feed marks at $1000\times$ that may have a possibility of being overlooked. At the same time, the height fluctuation degree of surface topography gradually becomes flat. Ultimately, leading to a decrease in surface irregularity and self-similarity, as well as a decrease in the fractal dimension values.

However, the variation trend of fractal dimension D with milling parameters does not change with the observation scales, which means that the variation trend of some inherent properties on the Ti-6Al-4V alloy surface caused by milling parameters, such as irregularity and self-similarity, are independent of the observation scale. And the variation trend of inherent properties on the Ti-6Al-4V alloy surface can be accurately described by the numerical changes of fractal dimension. Obviously, this makes up for the lack of roughness parameter characterization which depends on observation scales, equipment resolution, and sampling length.

5. Conclusion

This paper studied the multi-scale surface topography properties of Ti-6Al-4V alloy in peripheral milling. Milling experiments of Ti-6Al-4V titanium alloy were carried out based on the Taguchi method under different factors, including spindle speed n , radial depth of cut a_e , and feed rate f . The peripheral milling surface topographies at different scales were observed and quantitatively analyzed by using roughness parameters and fractal analysis. Conclusions were drawn as follows.

- (1) Surface defects in peripheral milling of Ti-6Al-4V alloy include feed marks, adhered material particles, scratches,

and cracks, etc. The spacing between adjacent feed marks perpendicular to the feed direction is affected by the feed rate. And the scratches caused by the milling tool clearance angle are located between adjacent feed marks. Adhered material particles are mainly formed by welding high-temperature microchips to the milling surface. Randomly unoriented scratches are caused by built-up edges or microchips sliding on the surface. And cracks are due to high levels of thermal and mechanical stress in the machining zone. According to the formation mechanism and distribution features, feed marks and scratches caused by the clearance angle are categorized as natural defects, and adhered material particles, random scratches and cracks are categorized as random defects.

- (2) At the observation scale of $200\times$ and $400\times$, surface roughness R_a , R_z , and S_a first decrease and then increase with the spindle speed n increasing, first increase and then decrease with the radial depth of cut a_e and feed rate f increasing. Lower roughness values are obtained at $n = 900$ rev/min, $a_e = 0.5$ mm, and $f = 0.06$ mm/rev. However, all studied surface roughness exhibits high variability at $1000\times$, which can be attributed to the surface defects perpendicular to the feed direction. Besides, the kurtosis and skewness of the milling surface show that there are no extreme peaks and valleys and the milling surfaces have good functional properties.
- (3) The machined surface fractal dimension D of Ti-6Al-4V increases with the increase of spindle speed n , increases first and then decreases with the increase of radial depth of cut a_e , and decreases with the increase of feed rate f , among which feed rate f has the minimum effect. Larger fractal dimensions are obtained at $n = 1150$ rev/min, $a_e = 0.3$ mm, and $f = 0.06$ mm/rev, where the surface structure is the most complex due to surface defects. Although the value of fractal dimension D changes with the observation scales, the variation trend with milling parameters does not change with it. This means that the variation trend with peripheral milling parameters of the fractal characteristics on the Ti-6Al-4V alloy surface, such as irregularity and self-similarity, is independent of the observation scale, equipment resolution, and sampling length.

Acknowledgments

The authors gratefully acknowledge the financial support from the National Natural Science Foundation of China (No. 52005002) and the Major Project of Anhui Provincial Department of Education (No.2023AH040010).

Conflict of interest

The authors declare that there are no conflicts of interest regarding the publication of this paper.

References

1. R.R. Boyer, *Titanium and Its Alloys: Metallurgy, Heat Treatment and Alloy Characteristics*, Encyclopedia of Aerospace Engineering, Wiley, Hoboken, 2010

2. M. Hourmand, A.A.D. Sarhan, M. Sayuti, and M. Hamdi, A Comprehensive Review on Machining of Titanium Alloys, *Arab. J. Sci. Eng.*, 2021, **46**(8), p 7087–7123
3. H. Mao, L. Jiao, S. Gao, J. Yi, Z. Peng, Z. Liu, P. Yan, and X. Wang, Surface Quality Evaluation in Meso-Scale End-Milling Operation Based on Fractal Theory and the Taguchi Method, *Int. J. Adv. Manuf. Tech.*, 2017, **91**(1), p 657–665
4. G. Sur, A.R. Motorcu, and S. Nohutçu, Single and Multi-objective Optimization for Cutting Force and Surface Roughness in Peripheral Milling of Ti6Al4V Using Fixed and Variable Helix Angle Tools, *J. Manuf. Process.*, 2022, **80**, p 529–545
5. D. Yang and Z. Liu, Surface Topography Analysis and Cutting Parameters Optimization for Peripheral Milling Titanium Alloy Ti-6Al-4V, *Int. J. Refract. Met. Hard Mat.*, 2015, **51**, p 192–200
6. N.W. Paschoalino, G.F. Batalha, E.C. Bordinassi, J.A.G. Ferrer, A.F. de Lima, G.D.X. Ribeiro, and C. Cardoso, MQL Strategies Applied in Ti-6Al-4V Alloy Milling—Comparative Analysis between Experimental Design and Artificial Neural Networks, *Materials*, 2020, **13**(17), p 3828
7. S. Wojciechowski, P. Twardowski, M. Pelic, R.W. Maruda, S. Barrans, and G.M. Krolczyk, Precision Surface Characterization for Finish Cylindrical Milling with Dynamic Tool Displacements Model, *Precis. Eng.*, 2016, **46**, p 158–165
8. R. Zhou and Q. Chen, An Analytical Prediction Model of Surface Topography Generated in 4-Axis Milling Process, *Int. J. Adv. Manuf. Tech.*, 2021, **115**(9), p 3289–3299
9. Q.R. Zeng, Y. Qin, W.L. Chang, and X.C. Luo, Correlating and Evaluating the Functionality-Related Properties with Surface Texture Parameters and Specific Characteristics of Machined Components, *Int. J. Mech. Sci.*, 2018, **149**, p 62–72
10. P. Karmiris-Obratański, N.E. Karkalos, R. Kudelski, and A.P. Markopoulos, Experimental Study on the Effect of the Cooling Method on Surface Topography and Workpiece Integrity During Trochoidal End Milling of Incoloy 800, *Tribol. Int.*, 2022, **176**, p 107899
11. V. Molnar and G. Szabo, Designation of Minimum Measurement Area for the Evaluation of 3D Surface Texture, *J. Manuf. Process.*, 2022, **83**, p 40–48
12. B. Yan, L. Zhu, and C. Liu, Prediction Model of Peripheral Milling Surface Geometry Considering Cutting Force and Vibration, *Int. J. Adv. Manuf. Tech.*, 2020, **110**(5), p 1429–1443
13. E. Ekici and G. Uzun, Effects on Machinability of Cryogenic Treatment Applied to Carbide Tools in the Milling of Ti6Al4V with Optimization Via the Taguchi Method and Grey Relational Analysis, *J. Braz. Soc. Mech. Sci. Eng.*, 2022, **44**(7), p 270
14. I.A. Daniyan, I. Tlhabadira, K. Mpofo, and R. Muvunzi, Numerical and Experimental Analysis of Surface Roughness during the Milling Operation of Titanium Alloy Ti6Al4V, *Int. J. Mech. Eng. Robot. Res.*, 2021, **10**(12), p 683–693
15. C. Bandapalli, B.M. Sutaria, D.V. Bhatt, and K.K. Singh, Experimental Investigation and Estimation of Surface Roughness using ANN, GMDH & MRA models in High Speed Micro End Milling of Titanium Alloy (Grade-5). 5th International Conference on Materials Processing and Characterization (ICMPC). Gokaraju Rangaraju Inst Engrg & Technol, Hyderabad, India, 2016
16. C. Bandapalli, B.M. Sutaria, and D.V. Bhatt, Estimation of Surface Roughness on Ti-6Al-4V in High Speed Micro End Milling by ANFIS Model, *Indian J. Eng. Mater. Sci.*, 2019, **26**(5–6), p 379–389
17. C. Bandapalli, K.K. Singh, B.M. Sutaria, and D.V. Bhatt, Experimental Investigation of Machinability Parameters in High-Speed Micro-End Milling of Titanium (grade-2), *Int. J. Adv. Manuf. Tech.*, 2016, **85**(9), p 2139–2153
18. C. Bandapalli, B.M. Sutaria, and D.V. Bhatt, Experimental Investigation of Surface Roughness in High-Speed Micro end Milling of Near Alpha Titanium Alloy, *Int. J. Precis. Technol.*, 2017, **7**(2–4), p 87–102
19. A. Molinari, S. Ancellotti, V. Fontanari, E. Iacob, V. Luchin, G. Zappini, and M. Benedetti, Effect of Process Parameters on the Surface Microgeometry of a Ti6Al4V Alloy Manufactured by Laser Powder Bed Fusion: 3D vs. 2D Characterization, *Metals*, 2022, **12**(1), p 106
20. L. Lizzul, M. Sorgato, R. Bertolini, A. Ghiotti, and S. Bruschi, Anisotropy Effect of Additively Manufactured Ti6Al4V Titanium Alloy on Surface Quality After Milling, *Precis. Eng.-J. Int. Soc. Precis. Eng. Nanotechnol.*, 2021, **67**, p 301–310
21. K. Aslantas, L.K.H. Alatrushi, F. Bedir, Y. Kaynak, and N. Yilmaz, An Experimental Analysis of Minimum Chip Thickness in Micro-Milling of Two Different Titanium Alloys, *Proc. Inst. Mech. Eng. Part B J. Eng. Manuf.*, 2020, **234**(12), p 1486–1498
22. B. Zhao, P.T. Li, C.Y. Zhao, and X.B. Wang, Fractal Characterization of Surface Microtexture of Ti6Al4V Subjected to Ultrasonic Vibration Assisted Milling, *Ultrasonics*, 2020, **102**, p 106052
23. H.J. Mao, L. Jiao, S.F. Gao, J. Yi, Z.X. Peng, Z.B. Liu, P. Yan, and X.B. Wang, Surface Quality Evaluation in Meso-Scale End-Milling Operation Based on Fractal Theory and the Taguchi Method, *Int. J. Adv. Manuf. Technol.*, 2017, **91**(1–4), p 657–665
24. Z. Niu, L. Jiao, S. Chen, P. Yan, and X. Wang, Surface Quality Evaluation in Orthogonal Turn-Milling Based on Box-Counting Method for Image Fractal Dimension Estimation, *Nanomanuf. Metrol.*, 2018, **1**(2), p 125–130
25. H.J. Cao, L. Liu, B. Wu, Y. Gao, and D. Qu, Process Optimization of High-Speed Dry Milling UD-CF/PEEK Laminates Using GA-BP Neural Network, *Compos. Pt. B-Eng.*, 2021, **221**, p 109034
26. X.K. Mu, W. Sun, C. Liu, B. Yuan, Y.L. Wang, and Q.C. Sun, Numerical Simulation and Accuracy Verification of Surface Morphology of Metal Materials Based on Fractal Theory, *Materials*, 2020, **13**(18), p 4158
27. D. Qu, B. Wang, and Z. Peng, The Influence of Processing Parameters on Surface Characteristics in Micro-Milling Thin-Walled Slot on Elgiloy, *Int. J. Adv. Manuf. Tech.*, 2017, **92**(5), p 2843–2852
28. Z. Liao, A. la Monaca, J. Murray, A. Speidel, D. Ushmaev, A. Clare, D. Axinte, and R. M'Saoubi, Surface Integrity in Metal Machining—Part I: Fundamentals of Surface Characteristics and Formation Mechanisms, *Int. J. Mach. Tools Manuf.*, 2021, **162**, p 103687
29. A. Gujrati, A. Sanner, S.R. Khanal, N. Moldovan, H. Zeng, L. Pastewka, and T.D.B. Jacobs, Comprehensive Topography Characterization of Polycrystalline Diamond Coatings, *Surf. Topogr.*, 2021, **9**(1), p 014003
30. C.A. Brown, H.N. Hansen, X.J. Jiang, F. Blateyron, J. Berglund, N. Senin, T. Bartkowiak, B. Dixon, G. Le Goic, Y. Quinsat, W.J. Stemp, M.K. Thompson, P.S. Ungar, and E.H. Zahouani, Multiscale Analyses and Characterizations of Surface Topographies, *CIRP Ann-Manuf. Technol.*, 2018, **67**(2), p 839–862
31. M.P. Fiorucci, A.J. Lopez, and A. Ramil, Multi-Scale Characterization of Topographic Modifications on Metallic Biomaterials Induced by Nanosecond Nd:YVO4 Laser Structuring, *Precis. Eng.-J. Int. Soc. Precis. Eng. Nanotechnol.*, 2018, **53**, p 163–168
32. T. Jana, A. Mitra, and P. Sahoo, Dynamic Contact Interactions of Fractal Surfaces, *Appl. Surf. Sci.*, 2017, **392**, p 872–882
33. X.H. Zhang, Y. Xu, and R.L. Jackson, An Analysis of Generated Fractal and Measured Rough Surfaces in Regards to Their Multi-Scale Structure and Fractal Dimension, *Tribol. Int.*, 2017, **105**, p 94–101
34. R. Piasecki, Detecting Self-Similarity in Surface Microstructures, *Surf. Sci.*, 2000, **454–456**, p 1058–1062
35. R.S. Sayles and T.R. Thomas, Surface Topography as a Nonstationary Random Process, *Nature*, 1978, **271**(5644), p 431–434
36. B.B. Mandelbrot, *Fractals and Chaos: The Mandelbrot Set and Beyond*, Springer, New York, 2004
37. P. Karolczak, M. Kowalski, and K. Raszka, Assessment of the Possibility of Using Fractal Analysis to Describe the Surface of Aluminum Composites After Turning, *Adv. Sci. Technol-Res.*, 2021, **15**(4), p 49–60
38. P. Wang, Q.S. Bai, K. Cheng, L. Zhao, and H. Ding, Optimization of the Process Parameters for Micro-Milling Thin-Walled Micro-Parts Using Advanced Algorithms, *Int. J. Adv. Manuf. Technol.*, 2022, **121**(9–10), p 6255–6269
39. G.P. Petropoulos, C.N. Pandazaras, and J.P. Davim, *Surface Texture Characterization and Evaluation Related to Machining*, Surface Integrity in Machining, Springer, London, 2010, p 37–66
40. ISO 4287 2009: Geometrical Product Specifications (GPS)—Surface texture: Profile method—Terms, definitions and surface texture parameters AMENDMENT 1: Peak count number
41. ISO 25178-2 2021: Geometrical product specifications (GPS)—Surface texture: Areal-Part 2: Terms, definitions and surface texture parameters
42. J.C. Russ, *Fractal Surfaces*, Springer, New York, 1994
43. T. Ai, R. Zhang, H.W. Zhou, and J.L. Pei, Box-Counting Methods to Directly Estimate the Fractal Dimension of a Rock Surface, *Appl. Surf. Sci.*, 2014, **314**, p 610–621

44. B. Dubuc, J.F. Quiniou, C. Roques-Carnes, C. Tricot, and S.W. Zucker, Evaluating the Fractal Dimension of Profiles, *Phys. Rev. A*, 1989, **39**(3), p 1500–1512
45. F. Feng, B.B. Liu, X.S. Zhang, X. Qian, X.H. Li, J.L. Huang, T.M. Qu, and P.F. Feng, Roughness Scaling Extraction Method for Fractal Dimension Evaluation Based on a Single Morphological Image, *Appl. Surf. Sci.*, 2018, **458**, p 489–494
46. H. Zhu, S. Ge, X. Huang, D. Zhang, and J. Liu, Experimental Study on the Characterization of Worn Surface Topography with Characteristic Roughness Parameter, *Wear*, 2003, **255**(1–6), p 309–314
47. S. Kulesza and M. Bramowicz, A Comparative Study of Correlation Methods for Determination of Fractal Parameters in Surface Characterization, *Appl. Surf. Sci.*, 2014, **293**, p 196–201
48. The Kennametal Web, <https://www.kennametal.com/cn/zh/home.html>. Accessed 2 November 2023
49. ISO 25178-3 2012: Geometrical product specifications (GPS) - Surface texture: Areal—Part 3: Specification operators
50. D. Ulutan and T. Ozel, Machining Induced Surface Integrity in Titanium and Nickel Alloys: A Review, *Int. J. Mach. Tools Manuf.*, 2011, **51**(3), p 250–280
51. A. Ginting and M. Nouari, Surface Integrity of Dry Machined Titanium Alloys, *Int. J. Mach. Tools Manuf.*, 2009, **49**(3), p 325–332
52. X. Liang, Z. Liu, and B. Wang, State-of-the-Art of Surface Integrity Induced by Tool Wear Effects in Machining Process of Titanium and Nickel Alloys: A Review, *Measurement*, 2019, **132**, p 150–181
53. S. Masoudi, M.J. Esfahani, F. Jafarian, and S.A. Mirsoleimani, Comparison the Effect of MQL, Wet and Dry Turning on Surface Topography, Cylindricity Tolerance and Sustainability, *Int. J. Precis Eng Manuf-Green Technol.*, 2023, **10**(1), p 9–21
54. S. Carvalho, A. Horovistiz, and J.P. Davim, Surface Topography in Machining Ti Alloys for Biomedical Applications: Correlative Microscopy Approach for Qualitative and Quantitative Analysis, *Int. J. Adv. Manuf. Technol.*, 2021, **114**(3–4), p 683–694
55. Y.L. Ke, H.Y. Dong, G. Liu, and M. Zhang, Use of Nitrogen Gas in High-Speed Milling of Ti-6Al-4V, *Trans. Nonferrous Met. Soc. China*, 2009, **19**(3), p 530–534
56. I. Ullah, S. Zhang, Q. Zhang, and B.X. Li, Microstructural and Mechanical Property Investigation of Machined Surface Layer in High-Speed Milling of Ti-6Al-4V Alloy, *Int. J. Adv. Manuf. Technol.*, 2021, **116**(5–6), p 1707–1719
57. H.X. Zhang, J. Zhao, F.Z. Wang, J.B. Zhao, and A.H. Li, Cutting Forces and Tool Failure in High-Speed Milling of Titanium Alloy TC21 with Coated Carbide Tools, *Proc. Inst. Mech. Eng. Part B-J. Eng. Manuf.*, 2015, **229**(1), p 20–27
58. S. Sun, M. Brandt, and M.S. Dargusch, Characteristics of Cutting Forces and Chip Formation in Machining of Titanium Alloys, *Int. J. Mach. Tools Manuf.*, 2009, **49**(7), p 561–568
59. M. Luo and Q. Yao, Vibrations of Flat-End Cutter Entering Workpiece Process: Modeling, Simulations, and Experiments, *Shock Vib.*, 2018, **2018**, p 8419013
60. Z. Chen, C.Z. Huang, B.H. Li, G.Y. Jiang, Z.Y. Tang, J.H. Niu, and H.L. Liu, Experimental Study on Surface Integrity of Inconel 690 Milled by Coated Carbide Inserts, *Int. J. Adv. Manuf. Technol.*, 2022, **121**(5–6), p 3025–3042
61. W.G. Song, Z.Q. Liu, G.H. Yao, A.M. Khan, and Y.K. Cai, Effect of Workpiece Work Hardening on Machined Surface Topography Generated in Two-Step Milling Process, *J. Manuf. Process.*, 2022, **77**, p 348–360
62. H. Guleryuz and H. Cimenoglu, Oxidation of Ti-6Al-4V Alloy, *J. Alloys Compd.*, 2009, **472**(1), p 241–246
63. Y. Meng, M. Villa, K.V. Dahl, B. Wang, M. Drouet, J.-B. Dubois, M.A.J. Somers, and T.L. Christiansen, Thermochemical Surface Hardening of Ti-6Al-4V: On the Role of Temperature and Treatment Media, *Surf. Coat. Technol.*, 2021, **422**, p 127505
64. S. Zhu, M. Zhao, J. Mao, and S.Y. Liang, A Ti-6Al-4V Milling Force Prediction Model Based on the Taylor Factor Model and Microstructure Evolution of the Milling Surface, *Micromachines*, 2022, **13**(10), p 1618
65. K. Gutzeit, G. Bulun, G. Stelzer, B. Kirsch, J. Seewig, and J.C. Aurich, Sub-Zero Milling of Ti-6Al-4V—impact of the Cutting Parameters on the Resulting Forces, Tool Wear, and Surface Quality, *Int. J. Adv. Manuf. Tech.*, 2023, **126**(7), p 3367–3381

Publisher's Note Springer Nature remains neutral with regard to jurisdictional claims in published maps and institutional affiliations.

Springer Nature or its licensor (e.g. a society or other partner) holds exclusive rights to this article under a publishing agreement with the author(s) or other rightsholder(s); author self-archiving of the accepted manuscript version of this article is solely governed by the terms of such publishing agreement and applicable law.